

## Distribution of *n*-alkanes in Miocene loess in Qinan, western Chinese Loess Plateau, and its palaeoenvironmental implications

SHEN JiaHeng<sup>1,2\*</sup>, XIAO GuoQiao<sup>3</sup>, WANG ZhiXiang<sup>3</sup>, SUN Qing<sup>4</sup>, WU HaiBin<sup>1,2</sup>,  
ZHANG ChunXia<sup>1,5</sup> & GUO ZhengTang<sup>1,2,5</sup>

<sup>1</sup> Key Laboratory of Cenozoic Geology and Environment, Institute of Geology and Geophysics, Chinese Academy of Sciences, Beijing 100029, China;

<sup>2</sup> University of Chinese Academy of Sciences, Beijing 100049, China;

<sup>3</sup> State Key Laboratory of Biogeology and Environmental Geology, School of Earth Sciences, China University of Geosciences, Wuhan 430074, China;

<sup>4</sup> National Research Center of Geoanalysis, Beijing 100037, China;

<sup>5</sup> Chinese Academy of Sciences Center for Excellence in Tibetan Plateau Earth Sciences, Beijing 100101, China

Received June 21, 2016; accepted February 15, 2017; published online March 22, 2017

**Abstract** Neogene eolian successions are one of the most important terrestrial palaeoenvironmental archives in East Asia. However, they have received far less attention than Quaternary loess deposits, especially in the case of lipid biomarker analysis. In order to obtain a better insight into the early-middle Miocene palaeoenvironment, we conducted a study of *n*-alkane biomarkers from sediments of the QA-I section (Qinan) in the western Chinese Loess Plateau, and compared the results with those of previous *n*-alkane analyses of eolian and aquatic sediments of varying age. Our principal results are as follows: (1) All QA-I samples contain *n*-alkanes ranging from C<sub>14</sub> to C<sub>35</sub>, among which the relative content of short-chain *n*-alkanes (C<sub>14</sub>–C<sub>20</sub>) from microorganisms is significantly greater than that of long-chain *n*-alkanes (C<sub>26</sub>–C<sub>35</sub>) from the waxes of terrestrial higher plants; the main peak is at C<sub>16</sub>–C<sub>18</sub>. All samples have a relatively lower abundance of medium-chain *n*-alkanes (C<sub>21</sub>–C<sub>25</sub>) than that of long- and short-chain *n*-alkanes, similar to strongly weathered palaeosols in Quaternary loess and Late Miocene-Pliocene Hipparion Red-Earth; however, this distribution is significantly different from that in weakly-weathered loess of Quaternary loess and Late Miocene-Pliocene Hipparion Red-Earth, as well as from aquatic sediments. (2) Despite some odd-over-even carbon predominance of long-chain *n*-alkanes in the QA-I samples, the carbon preference index (CPI) values are significantly lower than those of most of the weakly-weathered sediments. Our results show that strong weathering and microbial processes have significantly altered the *n*-alkanes in the Miocene eolian deposits in Qinan, and led to a significant oxidation and degradation of long-chain *n*-alkanes and the predominance of short-chain *n*-alkanes from bacteria. Therefore, the contribution of microorganism to total organic carbon (TOC) and its resulting in carbon isotopic composition should be carefully assessed in future studies.

**Keywords** Miocene, Loess, *n*-alkane, Palaeoenvironment, Qinan

**Citation:** Shen J H, Xiao G Q, Wang Z X, Sun Q, Wu H B, Zhang C X, Guo Z T. 2017. Distribution of *n*-alkanes in Miocene loess in Qinan, western Chinese Loess Plateau, and its palaeoenvironmental implications. *Science China Earth Sciences*, 60: 921–928, doi: 10.1007/s11430-016-9013-6

### 1. Introduction

The long, continuous sequences of eolian loess-soil deposits

in China are one of the most important continental palaeoenvironmental archives (Liu and Ding, 1998; Liu, 2009). Since the 1980s, significant progress has been made in understanding the course of late Neogene environmental evolution in Asia from systematic studies of late Miocene-Pliocene Hipparion Red-Earth and Quaternary loess deposits. Various

\* Corresponding author (email: shenjiaheng@mail.iggcas.ac.cn)

analytical approaches have been used, including pedology, environmental magnetism, sedimentology, geochemistry, and palaeontology (e.g., Liu and Ding, 1998; Liu, 2009; An, 2014). Recently, continuous eolian sequences spanning the interval from 22–3.5 Ma have been discovered in the western Chinese Loess Plateau (Guo et al., 2002, 2008; Hao and Guo, 2004, 2007; Zhan et al., 2011; Qiang et al., 2011; Ge et al., 2012). Analysis of these sequences has significantly improved our knowledge of the evolution of the East Asian monsoon system and of the process of Asian desertification over the last ~22 Ma. Important studies of the origin of the eolian deposits (Guo et al., 2002, 2010; Li et al., 2006a), stratigraphic framework (Guo et al., 2002; Hao and Guo, 2004, 2007; Qiang et al., 2011), spatial distribution (Yuan et al., 2007; Guo et al., 2008, 2010; Zhan et al., 2011; Ge et al., 2012), sedimentary characteristics (Liu et al., 2006; Qiao et al., 2006), geochemical composition (Guo et al., 2002; Liang et al., 2009), dust sources (Liang et al., 2014; Wang et al., 2017), rock-magnetic properties (Hao et al., 2008; Oldfield et al., 2009), snails (Li et al., 2006a, 2006b) and morphological properties (Guo et al., 2002) have been conducted on these continuous eolian sequences. However, in comparison with the Quaternary loess and red clay deposits, few detailed palaeoenvironmental and ecological studies of these sequences have been carried out because of their comparatively recent discovery.

Organic geochemistry is being increasingly applied to the study of global changes, with studies being conducted of organism-derived *n*-alkanes, fatty acids, fatty alcohols, fatty ketones, long-chain ketenes and GDGTs (glycerol dibiphytanyl glycerol tetraethers). In addition, increasing use is being made of compound-specific stable isotope analysis for palaeoenvironmental reconstruction (Eglinton and Eglinton, 2008). Among molecular fossils indicators, *n*-alkanes are resistant to weathering and are in common in sediments; in addition, different chains of *n*-alkanes have specific biological sources and thus are also of palaeoenvironmental significance. More specifically, carbon preference index (CPI), average chain length (ACL),  $C_{29}/C_{31}$  (or  $C_{27}/C_{31}$ ) ratios and compound-specific isotope analysis of  $C_{29}$  or  $C_{31}$  have been used to reconstruct vegetation composition, drought occurrence, and temperature change from Quaternary loess deposits (Xie et al., 2002, 2003; Zhang et al., 2003, 2006; Liu and Huang, 2006; Zhang et al., 2008; Zhou et al., 2016) and red clay sequences (Bai et al., 2009). However, relatively little attempt has been made to apply this methodology to early-middle Miocene eolian sediments (Peng et al., 2012, 2016).

In this study, the eolian sediments of the Qinan QA-I section (Guo et al., 2002) in the western Chinese Loess Plateau were selected for organic geochemical analyses. We analyzed the *n*-alkane distribution patterns of typical early-middle Miocene loess and paleosol samples in order to provide improved insight into the early-middle Miocene

palaeoenvironment. We also made a comparison with previously published *n*-alkanes data from eolian (Hipparion Red-Earth, Quaternary loess and modern soils in the Loess Plateau) and aquatic sediments (lacustrine, peat, and swamp deposits) of various ages and climatic contexts.

## 2. Materials and methods

The QA-I section (105°27'E, 35°02'N) is located in Qinan county, Gansu province, China, and is a classic sequence of Miocene eolian deposits (Figure 1). The section is 253-m thick and includes about 230 reddish palaeosol layers. Detailed magnetostratigraphic studies and analyses of micromammalian fossils spanning the interval from 22–6.2 Ma have been conducted on the QA-I section (Guo et al., 2002). Based on a detailed section description and chronology given in Guo et al. (2002), we selected 7 representative early-middle Miocene loess and palaeosol samples (Table 1) from the QA-I section for *n*-alkane analysis.

Biomarker analyses are susceptible to contamination during sampling, pre-processing and measurement, especially in the case of strongly weathered and organic-poor sediments. Consequently, the following sampling protocol was used for the QA-I section: The 0.5–1 m surface layer of the profile was removed, and then sampling trenches were excavated to a depth of >1 m from the freshly exposed surface. Bulk samples uncontaminated by modern plant roots and unaffected by reworking by water were carefully collected and sealed by silver paper. Each sample consisted of more than 300 g to enable repeat measurements. In the laboratory, the samples were air dried and the surface layer removed, and then the sample was ground to pass a 100 mesh sieve and sealed in silver paper prior to analysis.

In order to assess data quality and consistency, all of the samples were analyzed in two laboratories independently: at the National Research Center of Geoanalysis, Beijing, by the first author (Test II); and at the State Key Laboratory of Bio-

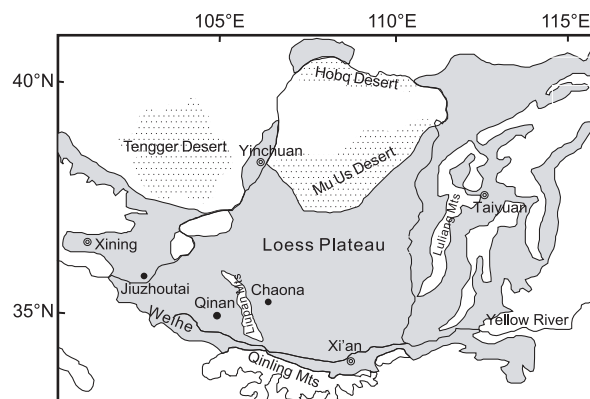


**Figure 1** The Chinese Loess Plateau and deserts in northern China together with the location of the QA-I section. Modified from Guo et al. (2008).

**Table 1** Sample information and *n*-alkane parameters of samples from the QA-I section

Sample ID	Depth (m)	Age (Ma)	Description	<i>L</i> (%)		CPI <sub>27-31</sub>	
				Test I	Test II	Test I	Test II
20ZW-36.25	75.00	~11.5	palaeosols	59.2	42.9	1.83	1.45
20QW-7.5	113.00	~13.7	palaeosols	64.6	58.2	2.32	1.64
99QW-177.25	167.25	~16.5	palaeosols	75.8	58.2	2.05	1.58
99QW-196	183.00	~17.1	loess	81.1	62.4	2.31	1.74
99QW-230.5	217.50	~20.0	palaeosols	76.5	57.1	2.30	2.04 <sup>b</sup>
99QW-340	240.00	~21.2	loess	78.6	67.0	2.39	1.77
99QW-348.5	248.50	~22.0	palaeosols	57.6	34.9	1.68	1.70

geology and Environmental Geology, China University of Geosciences, Wuhan, by the second author (Test I). Total lipids were extracted by using Soxhlet extraction and accelerated-solvent extraction (ASE100) (Willers et al., 2015) in two laboratories, respectively. About 20 g of sample was treated for 72 h with a solvent (Dichloromethane: Methanol, 9:1, v/v) using the Soxhlet extraction method. In the laboratory of China University of Geosciences, Wuhan, about 40 g of sample for each time was treated using ASE100, and repeated twice and then combined. The extracts were concentrated by evaporation to 1–2 mL, and then transferred to a small vial. After drying, the alkane fractions were separated with *n*-hexane via activated silica gel column chromatography.

To minimize contamination, all glassware was baked in a muffle furnace at 500°C for 6 hours and further rinsed with solvent before use. Blank samples were included in all measurements under identical experimental conditions to monitor possible contamination. After column chromatography, the alkane fractions were analyzed using a Shimadzu gas chromatograph (GC 2010) with DB-1 and Rtx-5 capillary columns, with helium as carrier gas at a flow rate of 1.7 mL/min. Individual *n*-alkanes were identified by comparison of retention time with a mixed standard of different carbon-number *n*-alkanes. The relative content of individual components was determined according to the integrated peak area and the calibration factor of the standard. The carbon preference index of long-chain *n*-alkane (CPI<sub>27-31</sub>)

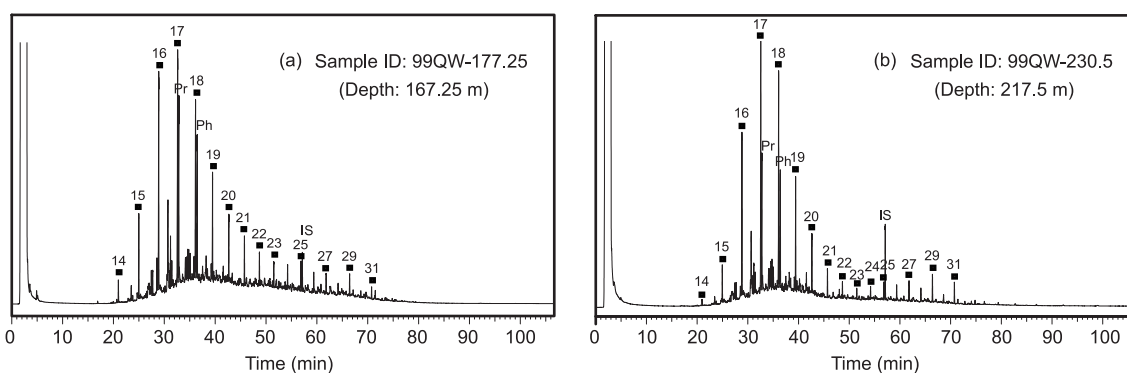
was calculated as follows (Peng et al., 2012):

$$\text{CPI}_{27-31} = 0.5 \times \left[ \frac{(C_{27} + C_{29} + C_{31})}{(C_{26} + C_{28} + C_{30})} + \frac{(C_{27} + C_{29} + C_{31})}{(C_{28} + C_{30} + C_{32})} \right]. \quad (1)$$

### 3. Results and discussion

#### 3.1 Distributions of *n*-alkanes

The biomarker results from the two independent laboratories are consistent in terms of the *n*-alkane distribution (Figures 2 and 3), except for one sample (99QW-348.5). However, there are some subtle differences in the content ratios of long-chain and short-chain *n*-alkanes. Both methods are well established and therefore they would not be expected to produce differences in *n*-alkane distributions (Willers et al., 2015). One reason for the inconsistency may be differences in experimental conditions and/or the low concentration of *n*-alkanes in the samples. When conducting Soxhlet extraction, only 20 g samples were extracted, which was less than the samples used for ASE100 (80 g). As a result, relatively less *n*-alkanes was obtained by Soxhlet extraction than ASE100, which could have resulted in relatively larger experimental errors than ASE method. The results for CPI<sub>27-31</sub> in Table 1 (Test I and II) demonstrate the influence of sample weight. The CPI<sub>27-31</sub> values are higher in Test I when the sample weight is larger, which indicates that when analyzing samples with a low abundance of molecular fossils, a significantly higher

**Figure 2** Gas chromatogram of *n*-alkanes in QA-I samples. IS, Internal standard.

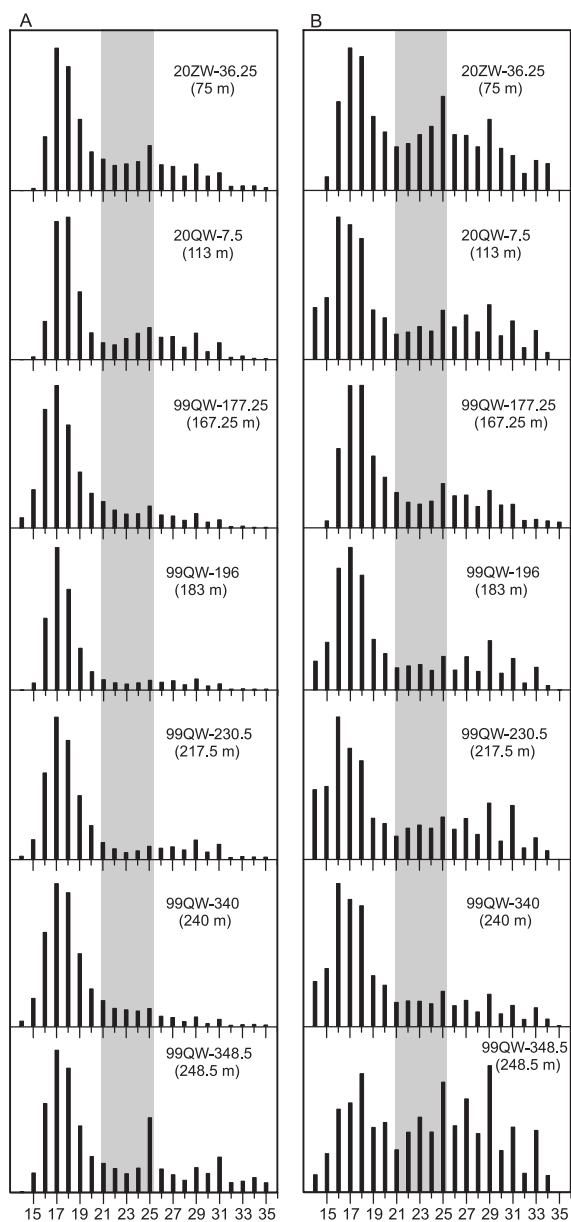


**Figure 3** Distribution patterns of *n*-alkanes in the QA-I samples. A and B are analysis results from the State Key Laboratory of Biogeology and Environmental Geology, China University of Geosciences, Wuhan, and the National Research Center of Geoanalysis, Beijing, respectively. The Y-axis is the relative abundance of different carbon numbers of *n*-alkanes.

sample weight should be used to maximize the reliability of the results.

Despite some subtle differences, the results from two laboratories have four main common characteristics (Figure 3): (1) The majority of the carbon numbers of *n*-alkanes are distributed within the range of  $C_{14}$ – $C_{35}$ . (2) The relative content of short-chain *n*-alkanes ( $C_{14}$ – $C_{20}$ ) ( $L$  (%)) is dominant in all samples (Table 1) with peaks at  $C_{16}$ – $C_{18}$ . There is no obvious odd-over even (or even-over odd) carbon predominance of short-chain *n*-alkanes. (3) Even though there is some odd carbon preference in long-chain *n*-alkanes, all of

the CPI values are very low (average of  $CPI_{27-31}$  is 2.13 and 1.70 from two laboratories, respectively). (4) In terms of relative content, most samples exhibit the highest abundance of short-chain *n*-alkanes ( $C_{14}$ – $C_{20}$ ), followed by long-chain *n*-alkanes ( $C_{21}$ – $C_{25}$ ), and medium-chain *n*-alkanes ( $C_{21}$ – $C_{25}$ ) have the lowest abundance. The results from the two independent laboratories are significantly different from those of Peng et al. (2012, 2016) which showed the highest abundance of medium-chain *n*-alkanes ( $C_{21}$ – $C_{25}$ ).

### 3.2 Palaeoenvironmental implications of the results

In order to assess the palaeoenvironmental significance of the *n*-alkanes record from the QA-I section, we compared our results with published data from sediments of different age and type and which had accumulated under different climatic conditions. Examples include the strongest and weakest developed palaeosols of the Hipparion Red-Earth in the Chaona section (Bai et al., 2009); the Quaternary loess ( $L_1$ ) and palaeosol ( $S_1$ ) layers in the Jiuzhoutai section near Lanzhou in northwest China (Xie et al., 2003); modern soil in arid grassland in the northern Chinese Loess Plateau (Luo et al., 2012); modern lacustrine sediments from Qinghai Lake (Duan et al., 2011); Eocene lacustrine sediment in Xining Basin (Xiao, 2013); Early Miocene lacustrine sediments in Linxia Basin (Wang et al., 2012); Holocene peats from Dajihu, Shennongjia, Hubei province (Huang et al., 2014a); and Holocene marsh sediments from Dadiwan, Qinan (Zhong et al., 2007) (Figure 4).

As shown in Figure 4, the distribution patterns of *n*-alkanes in the QA-I section are similar to those of the strongly weathered palaeosol (sample CN-5) of a Hipparion Red-Earth sequence (Bai et al., 2009) and a Quaternary palaeosol  $S_1$  (Samples 1–10) (Xie et al., 2003). In all cases, the relative content is dominated by short-chain *n*-alkanes, rather than by medium or long-chain *n*-alkanes. In contrast, our *n*-alkane distribution patterns are inconsistent with those of the weakly weathered palaeosol layer (sample CN-9) from a Hipparion Red-Earth sequence (Bai et al., 2009), Quaternary loess  $L_1$  (Samples 1–8) (Xie et al., 2003) and the modern soil from arid grassland in the northern Loess Plateau (Luo et al., 2012), which exhibit high abundances of short and long-chain *n*-alkanes and bimodal patterns (Figure 4c, e, f). Furthermore, the distribution of *n*-alkanes in QA-I section is clearly distinct from that of aquatic sediments (Figure 4g–k), including Eocene and Early Miocene lacustrine deposits, which exhibit higher abundances of long-chain *n*-alkanes and an odd-over-even carbon preference of long-chain *n*-alkanes (average  $CPI_{25-33}$  is 4.5).

Previous studies have shown that the distribution of *n*-alkanes from microorganisms is dominated by  $C_{15}$ – $C_{20}$  with the main peak at  $C_{17}$ – $C_{19}$ , and with no obvious odd-over-even carbon preference (Han and Calvin, 1969). The medium-chain

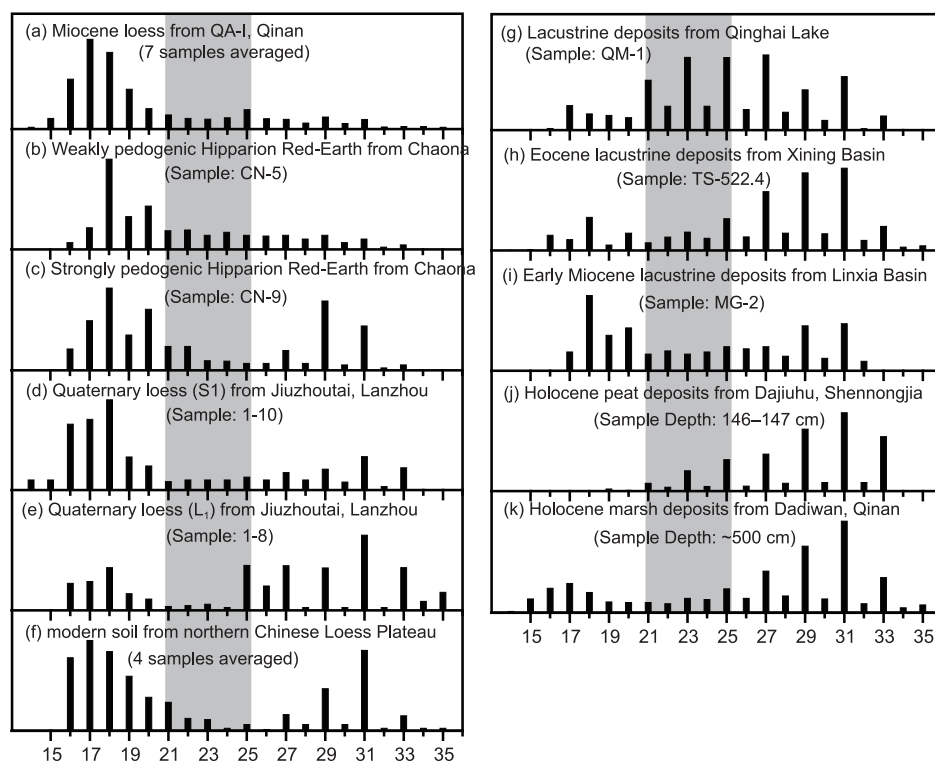


**Figure 4** Comparison of  $n$ -alkane distribution patterns between the QA-I samples and samples from representative eolian and aquatic sediments of contrasting age. The ordinate represents the relative content of different carbon-number  $n$ -alkanes in the samples. (a) Miocene loess from QA-I; (b)–(c) palaeosols of the Hipparion Red-Earth from Chaona (Bai et al., 2009); (d)–(e) Quaternary loess from Jiuzhoutai, Lanzhou (Xie et al., 2003); (f) modern soil in the northern Loess Plateau (Luo et al., 2012); (g) lacustrine deposits from Qinghai Lake (Duan et al., 2011); (h) Eocene lacustrine deposits in Xining Basin (Xiao, 2013); (i) Early Miocene lacustrine deposits in Linxia Basin (Wang et al., 2012); (j) a Holocene peat deposit from Dajiuahu, Shennongjia (Huang et al., 2014a); (k) Holocene marsh deposits from Dadiwan, Qinan (Zhong et al., 2007).

alkanes from submerged/floating-leaved aquatic macrophytes and *Sphagnum*, with a main peak at  $C_{23}$ – $C_{25}$ , have the highest abundance (Baas et al., 2000; Ficken et al., 2000; Huang et al., 2014b). In addition, the distributions of  $n$ -alkanes from the leaf wax of terrestrial plants are dominated by  $C_{27}$ ,  $C_{29}$ ,  $C_{31}$  and  $C_{33}$  with odd-over-even carbon preference of the long-chain  $n$ -alkanes ( $C_{26}$ – $C_{35}$ ) where the CPI values are generally greater than 5 (Eglinton and Hamilton, 1967; Rielley et al., 1991).

It is clear that in the eolian deposits the short-chain  $n$ -alkanes are mainly from microorganisms (Figure 4a–f), while the long-chain  $n$ -alkanes are produced by terrestrial plants. The abundance is lower in the medium-chain alkanes, which may reflect a mixture of sources from terrestrial plants and microorganisms. This is because terrestrial plants and microorganisms not only produce long and short-chain  $n$ -alkanes, but also minor medium-chain  $n$ -alkanes (Han and Calvin, 1969; Eglinton and Hamilton, 1967; Rielley et al., 1991). However, in the case of the aquatic deposits, there are significant differences in the abundances of medium-chain  $n$ -alkanes ( $C_{21}$ – $C_{25}$ ) (Figure 4g–k); among them,  $C_{23}$  and  $C_{25}$  are dominant in the modern lacustrine sediments from Qinghai Lake, indicating that the main contribution of  $n$ -alkanes is from aquatic plants.

The relative abundance of long-chain  $n$ -alkanes from

strongly pedogenic samples (Hipparion Red-Earth sample CN-5 and Quaternary loess samples 1–10) is lower than that from weakly pedogenic samples (weakly pedogenic Hipparion Red-Earth sample CN-9, Quaternary  $L_1$  and modern soil from the northern Loess Plateau) (Figure 4b–f), while the relative abundance of short-chain  $n$ -alkanes from microorganisms is higher. The results for the QA-I samples are in agreement with this trend because they have been subject to strong pedogenesis (Liang et al., 2009) and the abundance of long-chain  $n$ -alkanes is lower.

The distribution of  $n$ -alkanes in the QA-I samples may also reflect long-term weathering and microbial processes. These alterations cause a decrease in the total organic content as a result of oxidation and a decrease in the CPI values of long-chain  $n$ -alkanes by microbial processes (Freeman and Colarusso, 2001; Xie et al., 2004a; Luo et al., 2012; Zhou et al., 2016). Pollen studies indicate that plant growth is enhanced during warm and humid intervals compared to cold and dry intervals (Sun et al., 1997; Wang et al., 2006; Hui et al., 2011; Zhou et al., 2016). In general, flourishing vegetation would produce more long-chain  $n$ -alkanes. However, our QA-I samples exhibit a low abundance of long-chain  $n$ -alkanes, which demonstrates that the long-chain  $n$ -alkanes generated from land plants during warm and humid intervals were

degraded by weathering and microbial processes. This is consistent with the results from the Hipparion Red-Earth in the Chaona section (Bai et al., 2009). In contrast, in the case of aquatic sediments, which have not been subjected to pedogenesis (Figure 4g–k), even in the Eocene and Miocene samples the long-chain *n*-alkanes were well preserved (Xiao, 2013; Wang et al., 2012). Therefore, we suggest that the main reason for the low abundance of long-chain *n*-alkanes in the QA-I section is the effect of weathering and microbial processes, rather than burial time.

The average CPI<sub>27–33</sub> value of the samples from the QA-I section (the average CPI<sub>27–33</sub> of Test I in Table 1 is 2.1) is lower than that of the Quaternary loess samples (the average of CPI<sub>27–33</sub> is greater than 3) (Xie et al., 2004a; Bai et al., 2009) and the modern soil from the Loess Plateau (the average of CPI<sub>27–33</sub> is greater than 10) (Luo et al., 2012). It has been shown that lower CPI values occur under warm and humid climatic conditions because of the effect of the resulting strong weathering and microbial processes (Luo et al., 2012). For example, the CPI values of Quaternary palaeosol layers are generally lower than those of loess layers (Xie et al., 2003; Xie et al., 2004b; Liu and Huang, 2006; Zhang et al., 2006); and the CPI values in the late Miocene-Pliocene Hipparion Red-Earth was the lowest during the warmest interval of 3.8–5.6 Ma (Bai et al., 2009). Furthermore, the CPI values in modern soils exhibit a significant negative relationship with mean annual temperature and precipitation (Rao et al., 2009; Luo et al., 2012). Therefore, the lower CPI values of the QA-I samples indicate a warm and humid climate in the western Loess Plateau during the early-middle Miocene. This conclusion is consistent with morphological and geochemical evidence (Guo et al., 2002; Liang et al., 2009) and is also consistent with early-Middle Miocene climate conditions indicated by the continental weathering record of East Asia (Wei et al., 2006) and the global marine oxygen isotope record (Zachos et al., 2008).

Finally, studies have shown that the decrease in long-chain *n*-alkanes CPI values may be caused by degradation by microorganisms. Although the contribution of microorganisms to *n*-alkanes consists mainly of the short-chain types, there may also be a contribution of some long-chain *n*-alkanes with no obvious odd-over-even carbon predominance (Han and Calvin, 1969; Volkman et al., 1998; Ladygina et al., 2006). These long-chain *n*-alkanes from microorganisms would significantly decrease CPI values if they were dominant. On the other hand, degradation of long-chain *n*-alkanes caused by the metabolic processes of microorganisms would result in the greater decomposition of *n*-alkanes with an odd carbon number compared with those with an even carbon number, thus causing a decrease in the CPI value (Wentzel et al., 2007; Luo et al., 2012). These two effects would be enhanced in humid and warm climates (Freeman and Colaruso, 2001; Xie et al., 2004a; Luo et al., 2012). There-

fore, our results suggest that microorganism blooms under the early-middle Miocene warm climate would not only provide abundance of short-chain *n*-alkanes, but also decrease CPI values by reducing the long-chain *n*-alkanes produced by higher plants and supplying long-chain *n*-alkanes with no obvious odd-over-even carbon predominance.

### 3.3 Implications of the results for carbon isotope measurements

The isotopic values of total organic carbon (TOC) from eolian sediments are often used to infer the palaeoclimate and palaeovegetation of the Loess Plateau (e.g. Xie et al., 2004a; Liu et al., 2007); however, the origin of organic materials in eolian sediments is complex (Xie et al., 2004a; Liu et al., 2007) and there are several sources: (1) organic materials provided by the growth of a local organism (mainly plants), (2) organic materials produced by local microorganisms in the process of soil formation, and (3) allochthonous organic materials transported from the dust source areas. Clearly, only the carbon isotopic values from local plants are of climatic/ecological significance.

The organic matter produced by microorganisms can affect the isotopic composition of total organic carbon (Huang et al., 1996; Zhang et al., 2003) due to the wide range of carbon isotopic values of the organic matter derived from microorganisms (Pancost and Sinninghe Damsté, 2003). In addition, allochthonous organic matter not only contains ‘old organic matter’ derived from the soil parent material, but also ‘new organic matter’ from higher plants and microorganisms in the dust source areas; thus it can also affect the isotopic values of TOC (Xie et al., 2004a; Liu et al., 2007). In most cases, such as modern soil and Quaternary loess, the very low proportions of the microbial and allochthonous organic matter would not significantly affect the carbon isotopic values of the TOC (e.g., Zhang et al., 2003; Rao et al., 2008; Zhou et al., 2016).

Our results indicate that the relative abundance of short-chain *n*-alkanes (*L* (%)) in the QA-I samples exceeds 50% (Table 1), indicating the organic matter from microorganisms may make the principal contribution to the TOC, which will consequently affect the interpretation of the palaeoclimate/palaeoecology by carbon isotopic composition of TOC. Recent studies suggest that, probably due to microbial activity, the carbon isotopic values of TOC are significantly different from those of pyrogenic carbon (Zhou et al., 2016). However, to date, it is difficult to quantify the effect of microbial organic matter on TOC and its carbon isotopic composition in different samples. In addition, because of the low abundance of *n*-alkanes, the proportion of allochthonous *n*-alkanes from soil parent material (CPI values close to 1) cannot be ignored (Xie et al., 2004a). High maturity *n*-alkanes have a high abundance of medium carbon numbers (Freeman

and Colarusso, 2001), which would contribute to the relative abundance of C<sub>25</sub> and C<sub>26</sub>. Therefore, in future studies the effect of allochthonous organic input should also be assessed when interpreting the carbon isotopic composition of TOC.

#### 4. Conclusions

We have measured the *n*-alkane distributions of typical loess and palaeosol from the early-middle Miocene QA-I section in Qinan, Gansu province, China, and compared our results with the *n*-alkanes distributions from different types of eolian and aquatic deposits. The main findings are as follows:

(1) The distributions of *n*-alkanes in the QA-I section range from C<sub>14</sub> to C<sub>35</sub>. Short-chain *n*-alkanes (C<sub>14</sub>–C<sub>20</sub>) from microorganisms have the highest abundance, followed by long-chain *n*-alkanes (C<sub>26</sub>–C<sub>35</sub>), and medium-chain *n*-alkanes (C<sub>21</sub>–C<sub>25</sub>) have the lowest abundance. The carbon peaks are between C<sub>16</sub>–C<sub>18</sub>. This distribution is consistent with results for strongly weathered palaeosols in Quaternary loess and Late Miocene-Pliocene Hipparion Red-Earth sequences, but is significantly different from that of weakly weathered eolian sediments and aquatic sediments.

(2) The abundance of *n*-alkanes and CPI values of long-chain alkanes in the QA-I section are lower than those in Eocene lacustrine deposits, Quaternary loess and modern soil. This indicates that the Miocene eolian deposits have experienced stronger weathering and microbial processes than Quaternary loess, which would have resulted in the dominance of short-chain *n*-alkanes from microorganisms due to the significant oxidation and degradation of long-chain *n*-alkanes. Our results indicate that organic matter from microorganisms made the largest contribution to the TOC of Miocene eolian deposits, with implications for the palaeoclimatic and palaeoecological interpretation of the stable carbon isotopic composition of TOC. In the case of sediments which have been significantly affected by microorganisms, the contribution of the organic matter from microorganisms to the carbon isotopic composition of TOC should be carefully assessed in the future.

**Acknowledgements** We are grateful to Associate Professor Xianyu Huang for his advice regarding the experiments and data analysis, two anonymous reviewers for their useful suggestions, and Professor Jan Bloemendal (at University of Liverpool of UK) for language editing. This study was financially supported by National Natural Science Foundation of China (Grant Nos. 41430531, 41202249 & 41125011) and the China Geological Survey (Grant No. 1212011121261).

#### References

An Z S. 2014. Late Cenozoic Climate Change in Asia: Loess, Monsoon and Monsoon-Arid Environment Evolution. Netherlands: Springer. 582  
Baas M, Pancost R, van Geel B, Sinninghe Damsté J S. 2000. A comparative study of lipids in Sphagnum species. *Org Geochem*, 31: 535–541

Bai Y, Fang X, Nie J, Wang Y, Wu F. 2009. A preliminary reconstruction of the paleoecological and paleoclimatic history of the Chinese Loess Plateau from the application of biomarkers. *Palaeogeogr Palaeoclimatol Palaeoecol*, 271: 161–169  
Duan Y, Wu B, Xu L, He J, Sun T. 2011. Characterisation of *n*-alkanes and their hydrogen isotopic composition in sediments from Lake Qinghai, China. *Org Geochem*, 42: 745–746  
Eglinton T I, Eglinton G. 2008. Molecular proxies for paleoclimatology. *Earth Planet Sci Lett*, 275: 1–16  
Eglinton G, Hamilton R J. 1967. Leaf epicuticular waxes. *Science*, 156: 1322–1335  
Ficken K J, Li B, Swain D L, Eglinton G. 2000. An *n*-alkane proxy for the sedimentary input of submerged/floating freshwater aquatic macrophytes. *Org Geochem*, 31: 745–749  
Freeman K H, Colarusso L A. 2001. Molecular and isotopic records of C<sub>4</sub> grassland expansion in the late miocene. *Geochim Cosmochim Acta*, 65: 1439–1454  
Guo Z T, Ge J Y, Xiao G Q, Hao Q Z, Wu H B, Zhan T, Liu L, Qin L, Zeng F M, Yuan B Y. 2010. Comment on “Mudflat/distal fan and shallow lake sedimentation (upper Vallesian-Turolian) in the Tianshui Basin, Central China: Evidence against the late Miocene eolian loess” by A. M. Alonso-Zarza, Z. Zhao, C. H. Song, J. J. Li, J. Zhang, A. Martín-Pérez, R. Martín-García, X. X. Wang, Y. Zhang and M.H. Zhang [*Sedimentary Geology* 222 (2009) 42–51]. *Sediment Geol*, 230: 86–89  
Guo Z T, Ruddiman W F, Hao Q Z, Wu H B, Qiao Y S, Zhu R X, Peng S Z, Wei J J, Yuan B Y, Liu T S. 2002. Onset of Asian desertification by 22 Myr ago inferred from loess deposits in China. *Nature*, 416: 159–163  
Guo Z T, Sun B, Zhang Z S, Peng S Z, Xiao G Q, Ge J Y, Hao Q Z, Qiao Y S, Liang M Y, Liu J F, Yin Q Z, Wei J J. 2008. A major reorganization of Asian climate by the early Miocene. *Clim Past*, 4: 153–174  
Ge J, Guo Z, Zhan T, Yao Z, Deng C, Oldfield F. 2012. Magnetostratigraphy of the Xihe loess-soil sequence and implication for late Neogene deformation of the West Qinling Mountains. *Geophys J Int*, 189: 1399–1408  
Han J, Calvin M. 1969. Hydrocarbon distribution of algae and bacteria, and microbiological activity in sediments. *Proc Natl Acad Sci USA*, 64: 436–443  
Hao Q, Guo Z. 2004. Magnetostratigraphy of a late Miocene-Pliocene loess-soil sequence in the western Loess Plateau in China. *Geophys Res Lett*, 31: L09209  
Hao Q, Guo Z. 2007. Magnetostratigraphy of an early-middle Miocene loess-soil sequence in the western Loess Plateau of China. *Geophys Res Lett*, 34: L18305  
Hao Q, Oldfield F, Bloemendal J, Guo Z. 2008. The magnetic properties of loess and paleosol samples from the Chinese Loess Plateau spanning the last 22 million years. *Palaeogeogr Palaeoclimatol Palaeoecol*, 260: 389–404  
Huang Y, Bol R, Harkness D D, Ineson P, Eglinton G. 1996. Post-glacial variations in distributions, <sup>13</sup>C and <sup>14</sup>C contents of aliphatic hydrocarbons and bulk organic matter in three types of British acid upland soils. *Org Geochem*, 24: 273–287  
Huang X, Meyers P A, Xue J, Wang X, Zheng L. 2014a. Cryptic abundance of long-chain iso and anteiso alkanes in the Dajiuhe peat deposit, central China. *Org Geochem*, 66: 137–139  
Huang X, Xue J, Meyers P A, Gong L, Wang X, Liu Q, Qin Y, Wang H. 2014b. Hydrologic influence on the δ<sup>13</sup>C variation in long chain *n*-alkanes in the Dajiuhe peatland, central China. *Org Geochem*, 69: 114–119  
Hui Z, Li J, Xu Q, Song C, Zhang J, Wu F, Zhao Z. 2011. Miocene vegetation and climatic changes reconstructed from a sporopollen record of the Tianshui Basin, NE Tibetan Plateau. *Palaeogeogr Palaeoclimatol Palaeoecol*, 308: 373–382  
Ladygina N, Dedyukhina E G, Vainshtein M B. 2006. A review on microbial synthesis of hydrocarbons. *Process Biochem*, 41: 1001–1014  
Li F J, Wu N Q, Pei Y P, Hao Q Z, Rousseau D D. 2006a. Wind-blown origin of Dongwan late Miocene-Pliocene dust sequence documented by land

- snail record in western Chinese Loess Plateau. *Geology*, 34: 405–408
- Li F J, Wu N Q, Rousseau D D. 2006b. Preliminary study of mollusk fossils in the Qinan Miocene loess-soil sequence in western Chinese Loess Plateau. *Sci China Ser D-Earth Sci*, 49: 724–730
- Liang M Y, Guo Z T, Kahmann A J, Oldfield F. 2009. Geochemical characteristics of the Miocene eolian deposits in China: Their provenance and climate implications. *Geochim Geophys Geosyst*, 10: Q04004
- Liang M, Wang Z, Zhou S, Zong K, Hu Z. 2014. The provenance of Gansu Group in Longxi region and implications for tectonics and paleoclimate. *Sci China Earth Sci*, 57: 1221–1228
- Liu J, Guo Z, Qiao Y, Hao Q, Yuan B. 2006. Eolian origin of the Miocene loess-soil sequence at Qin'an, China: Evidence of quartz morphology and quartz grain-size. *Chin Sci Bull*, 51: 117–120
- Liu T S, Ding Z L. 1998. Chinese loess and the paleomonsoon. *Annu Rev Earth Planet Sci*, 26: 111–145
- Liu T S. 2009. *Loess and Arid Environment*. Hefei: Anhui Science and Technology Press. 537
- Liu W G, Huang Y S. 2006. Compound specific D/H ratios and molecular distributions of higher plant leaf waxes as novel paleoenvironmental indicators in the Chinese Loess Plateau. *Org Geochem*, 36: 851–860
- Liu W, Yang H, Ning Y, An Z. 2007. Contribution of inherent organic carbon to the bulk  $\delta^{13}\text{C}$  signal in loess deposits from the arid western Chinese Loess Plateau. *Org Geochem*, 38: 1571–1579
- Luo P, Peng P A, Lü H Y, Zheng Z, Wang X. 2012. Latitudinal variations of CPI values of long-chain *n*-alkanes in surface soils: Evidence for CPI as a proxy of aridity. *Sci China Earth Sci*, 55: 1134–1146
- Oldfield F, Hao Q Z, Bloemendal J, Gibbs-Eggar Z, Patil S, Guo Z T. 2009. Links between bulk sediment particle size and magnetic grain-size: General observations and implications for Chinese loess studies. *Sedimentology*, 56: 2091–2106
- Pancost R D, Sinninghe Damsté J S. 2003. Carbon isotopic compositions of prokaryotic lipids as tracers of carbon cycling in diverse settings. *Chem Geol*, 195: 29–58
- Peng T, Li J, Song C, Guo B, Liu J, Zhao Z, Zhang J. 2016. An integrated biomarker perspective on Neogene-Quaternary climatic evolution in NE Tibetan Plateau: Implications for the Asian aridification. *Quat Int*, 399: 174–182
- Peng T, Li J, Song C, Zhao Z, Zhang J, Hui Z, King J W. 2012. Biomarkers challenge early Miocene loess and inferred Asian desertification. *Geophys Res Lett*, 39: L06702
- Qiang X, An Z, Song Y, Chang H, Sun Y, Liu W, Ao H, Dong J, Fu C, Wu F, Lu F, Cai Y, Zhou W, Cao J, Xu X, Ai L. 2011. New eolian red clay sequence on the western Chinese Loess Plateau linked to onset of Asian desertification about 25 Ma ago. *Sci China Earth Sci*, 54: 136–144
- Qiao Y S, Guo Z T, Hao Q Z, Yin Q Z, Yuan B Y, Liu T S. 2006. Grain-size features of a Miocene loess-soil sequence at Qinan: Implications on its origin. *Sci China Ser D-Earth Sci*, 49: 731–738
- Rao Z G, Jia G D, Zhu Z Y, Wu Y, Zhang J W. 2008. Comparison of the carbon isotope composition of total organic carbon and long-chain *n*-alkanes from surface soils in eastern China and their significance. *Chin Sci Bull*, 53: 3921–3927
- Rao Z, Zhu Z, Wang S, Jia G, Qiang M, Wu Y. 2009. CPI values of terrestrial higher plant-derived long-chain *n*-alkanes: A potential paleoclimatic proxy. *Front Earth Sci China*, 3: 266–272
- Rielley G, Collier R J, Jones D M, Eglinton G. 1991. The biogeochemistry of Ellesmere Lake, U.K.—I: Source correlation of leaf wax inputs to the sedimentary lipid record. *Org Geochem*, 17: 901–912
- Sun X J, Song C Q, Wang F Y, Sun M R. 1997. Vegetation history of the Loess Plateau of China during the last 100000 years based on pollen data. *Quat Int*, 37: 25–36
- Volkman J K, Barrett S M, Blackburn S I, Mansour M P, Sikes E L, Gelin F. 1998. Microalgal biomarkers: A review of recent research developments. *Org Geochem*, 29: 1163–1179
- Wang L, Lü H Y, Wu N Q, Li J, Pei Y P, Tong G B, Peng S Z. 2006. Palynological evidence for Late Miocene–Pliocene vegetation evolution recorded in the red clay sequence of the central Chinese Loess Plateau and implication for palaeoenvironmental change. *Palaeogeogr Palaeoclimatol Palaeoecol*, 241: 118–128
- Wang Y, Fang X, Zhang T, Li Y, Wu Y, He D, Gao Y, Meng P, Wang Y. 2012. Distribution of biomarkers in lacustrine sediments of the Linxia Basin, NE Tibetan Plateau, NW China: Significance for climate change. *Sediment Geol*, 243–244: 108–116
- Wang Z X, Liang M Y, Sun Y Q, Dai G W. 2017. Cenozoic tectonic and geomorphic evolution of the Longxi region in northeastern Tibetan Plateau interpreted from detrital zircon. *Sci China Earth Sci*, 60: 256–267
- Wei G, Li X H, Liu Y, Shao L, Liang X. 2006. Geochemical record of chemical weathering and monsoon climate change since the early Miocene in the South China Sea. *Paleoceanography*, 21: PA4214
- Wentzel A, Ellingsen T E, Kotlar H K, Zotchev S B, Throne-Holst M. 2007. Bacterial metabolism of long-chain *n*-alkanes. *Appl Microbiol Biotechnol*, 76: 1209–1221
- Willers C, Jansen van Rensburg P J, Claessens S. 2015. Microbial signature lipid biomarker analysis—An approach that is still preferred, even amid various method modifications. *J Appl Microbiol*, 118: 1251–1263
- Xiao G Q. 2013. *Biomarker records across the Eocene-Oligocene climate transition from the Xining Basin, Northwestern China*. Post-Doctoral Report. Wuhan: China University of Geosciences
- Xie S, Guo J, Huang J, Chen F, Wang H, Farrimond P. 2004a. Restricted utility of  $\delta^{13}\text{C}$  of bulk organic matter as a record of paleovegetation in some loess-Paleosol sequences in the Chinese Loess Plateau. *Quat res*, 62: 86–93
- Xie S C, Chen F H, Wang Z Y, Wang H M, Gu Y S, Huang Y S. 2003. Lipid distributions in loess-paleosol sequences from northwest China. *Org Geochem*, 34: 1071–1079
- Xie S C, Nott C J, Avsejs L A, Maddy D, Chambers F M, Evershed R P. 2004b. Molecular and isotopic stratigraphy in an ombrotrophic mire for paleoclimate reconstruction. *Geochim Cosmochim Acta*, 68: 2849–2862
- Xie S C, Wang Z Y, Wang H M, Chen F H, An C B. 2002. The occurrence of a grassy vegetation over the Chinese Loess Plateau since the last interglacier: The molecular fossil record. *Sci China Ser D-Earth Sci*, 45: 53–62
- Yuan B Y, Guo Z T, Hao Q Z, Peng S Z, Qiao Y S, Wu H B, Xiao G Q, Ge J Y, Sun B, Zhou X, Yin Q Z, Liang M Y, Qin L, Liu L, Yao Z Q, Liu T. 2007. Cenozoic evolution of geomorphic and sedimentary environments in the Tianshui-Qin'an regions (in Chinese). *Quat Sci*, 27: 161–171
- Zachos J C, Dickens G R, Zeebe R E. 2008. An early Cenozoic perspective on greenhouse warming and carbon-cycle dynamics. *Nature*, 451: 279–283
- Zhan T, Guo Z T, Wu H B, Ge J Y, Zhou X, Wu C L, Zeng F M. 2011. Thick Miocene eolian deposits on the Huajialing Mountains: The geomorphic evolution of the western Loess Plateau. *Sci China Earth Sci*, 54: 241–248
- Zhang H C, Yang M S, Zhang W X, Lei G L, Chang F Q, Pu Y, Fan H F. 2008. Molecular fossil and paleovegetation records of paleosol S4 and adjacent loess layers in the Luochuan loess section, NW China. *Sci China Ser D-Earth Sci*, 51: 321–330
- Zhang Z H, Zhao M X, Eglinton G, Lu H Y, Huang C Y. 2006. Leaf wax lipids as paleovegetational and paleoenvironmental proxies for the Chinese Loess Plateau over the last 170 kyr. *Quat Sci Rev*, 25: 575–594
- Zhang Z H, Zhao M X, Lu H Y, Faiia A M. 2003. Lower temperature as the main cause of C4 plant declines during the glacial periods on the Chinese Loess Plateau. *Earth Planet Sci Lett*, 214: 467–481
- Zhong Y X, Chen F H, An C B, Xie S C, Huang X Y. 2007. Holocene vegetation cover in Qin'an area of western Chinese Loess Plateau revealed by *n*-alkane. *Chin Sci Bull*, 52: 1692–1698
- Zhou B, Wali G, Peterse F, Bird M I. 2016. Organic carbon isotope and molecular fossil records of vegetation evolution in central Loess Plateau since 450 kyr. *Sci China Earth Sci*, 59: 1206–1215